Vibrational Substructure in the OH Stretching Transition of Water and HOD

Zhaohui Wang, Andrei Pakoulev, Yoonsoo Pang, and Dana D. Dlott*

School of Chemical Sciences, University of Illinois at Urbana−Champaign, 600 South Mathews Avenue, Urbana, Illinois 61801

Received: April 2, 2004; In Final Form: August 13, 2004

Ultrafast nonlinear vibrational spectroscopy with mid-IR pumping and incoherent anti-Stokes Raman probing is used to study $v = 1$ excitations of OH stretching (ν_{OH}) of water and of HOD in D_2O solvent (HOD/D_2O). The parent ν_{OH} decay and the appearance of daughter stretching and bending excitations are simultaneously monitored, which allows for characterization of the stretch decay pathways. At all times and with all pump frequencies within the ν_{OH} band, the excited-state spectrum can be fit by two overlapping subbands, a broader red-shifted band ν_{OH}^{R} and a narrower blue-shifted band ν_{OH}^{B}. We show these subbands are dynamically distinguishable. They decay with different lifetimes and evidence characteristically different decay pathways. Excitations of the ν_{OH}^{R} subband generate bending vibrations that ν_{OH}^{B} does not. The shorter lifetime (~0.5 ps) of the ν_{OH}^{R} subband compared to the ν_{OH}^{B} subband (0.8−0.9 ps) results primarily from enhanced stretch-to-bend anharmonic coupling. The subbands represent persistent structures in the excited state, in that interconversion between subbands (2−10 ps) is slower than excited-state decay. A tentative structural interpretation is proposed. The ν_{OH}^{R} subband, on the basis of simulations, its red shift ,and its shorter lifetime, is proposed to result from strongly hydrogen-bonded "ice-like" water. The ν_{OH}^{R} subband has a smaller amplitude in HOD/D_2O than in water, possibly because HOD has a single localized OH-stretching vibration whereas water has two delocalized stretching vibrations.

1. Introduction

In this work, we use ultrafast nonlinear vibrational spectroscopy to demonstrate that the OH-stretching (ν_{OH}) band of water consists of *two distinct subbands that evidence clearly distinguishable dynamical behavior*. A subband is a spectrally contiguous region within the ν_{OH} band that can be experimentally distinguished from other parts of the band. Here we measure the transient anti-Stokes Raman spectrum[1] of water and HOD solute in D_2O (HOD/D_2O) of ν_{OH} excitations in $v = 1$ generated by a tunable mid-IR pulse and probed via the $v = 1 \rightarrow 0$ Raman transition. We observe two overlapping subbands that are distinguishable by virtue of having different excited-state lifetimes and different vibrational relaxation (VR) pathways. The blue-shifted subband undergoes slower VR with minimal generation of δ_{H_2O} or δ_{HOD} bending excitations and the red-shifted subband undergoes faster VR with more efficient generation of bending excitations. Subbands of this type will be termed "dynamically distinguishable". In the past, most discussions of water subbands[2−4] has focused on the idea that if subbands exist, they should be attributed to characteristic hydrogen-bonding environments. Subbands of this type will be termed "structurally distinguishable". To the extent that we may associate different dynamics with different structures, our observations indicate that the two subbands represent water environments that are persistent in the sense that interconversion (estimated at 2−10 ps) is somewhat slower than the $v = 1$ excited-state lifetime of 0.5−1.0 ps. Thus our work suggests that a glass of water at ambient temperature consists of two distinct interconverting types of water molecules that behave in characteristically different ways. This dual structure is not at all what one expects on the basis of water simulations,[5] but a recent X-ray absorption and X-ray Raman study has been interpreted as indicating that water consists mainly of two hydrogen-bonded configurations.[5]

The ease of fitting water vibrational spectra in the ν_{OH} region by using a small number of overlapping Gaussian subbands has frequently been interpreted as an argument for the existence of interconverting structurally distinguishable subbands that represent different hydrogen-bonded structures,[2] for instance "ice-like" or "bridged" structures. However, Gaussian fitting of ultrabroadened vibrational spectra in hydrogen-bonded liquids is a poor tool for discerning structurally distinct elements. Recently developed techniques in ultrafast nonlinear vibrational spectroscopy[6] allow a much more effective attack on this problem with use of line narrowing or hole-burning methods.[6,7] These methods ought to permit a straightforward determination of the existence of dynamically distinguishable subbands. Making the connection to underlying structures is more difficult owing to the rather complicated relationship between the vibrational spectrum and local structure. Usually simulations are needed to make this connection, although some insight into this problem is gained in this work by a comparison of results from both water and HOD/D_2O.

Most prior experimental work in this area used ultrafast IR[3,4,8−21] or IR−Raman[22,23] methods to study ν_{OH} of HOD/D_2O. There have been far fewer studies of water[15,21,22,24−28] itself. Most of these works agree that the rates of VR and orientational relaxation vary within the ν_{OH} band. Some groups find that the HOD VR lifetime varies continuously across the band.[18] Our group[27] in a recent study of water found just two discrete lifetimes. The orientational relaxation rate in HOD is said to take on a small number of discrete values,[3,12] but if correct the

* To whom correspondence should be addressed. E-mail dlott@scs.uiuc.edu.

10.1021/jp048545t CCC: $27.50
Published on Web 09/25/2004

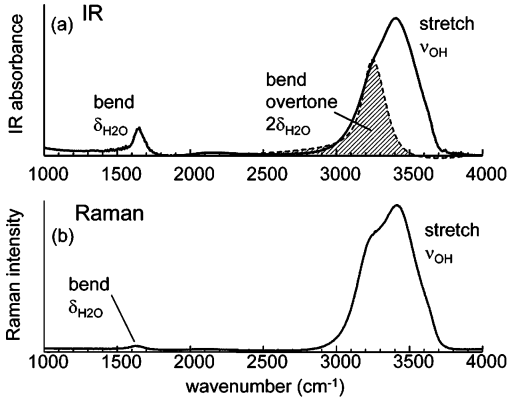

Figure 1. IR and Raman spectra of water, showing the OH-stretching (ν_{OH}) region and bending (δ_{H_2O}) region. The shaded region indicates the approximate location of the bend overtone $2\delta_{H_2O}$.

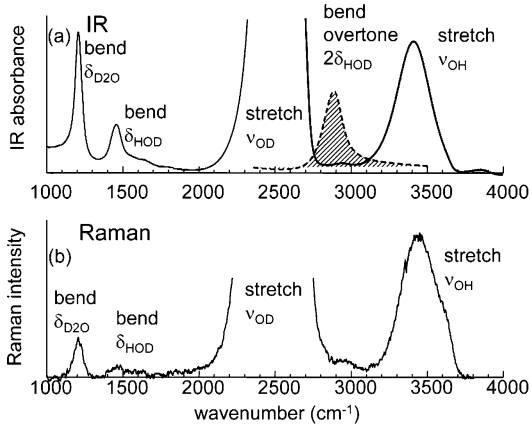

Figure 2. IR and Raman spectra of a 10% solution of HOD/D_2O. The OD stretching region has contributions from both HOD and D_2O. The shaded region indicates the approximate location of the bend overtone $2\delta_{HOD}$ transition.

actual number (either two[12] or three or more[3,12]) is not settled. The relevant experimental works will be described below, but we believe that it is fair to say that until now it is inconclusive whether these dynamical properties evidence a small number of discrete values or a continuous variation within the ν_{OH} band.

Computer simulations[29−36] have shown that a wide range of hydrogen-bonding parameters (lengths, angles, strengths, etc.) coexist in water and in HOD/D_2O, which appears to argue for a continuous distribution of properties. On the other hand, by using potentially arbitrary geometrical or energetic cutoff criteria to determine whether a particular atom participates in a hydrogen bond or not (e.g. refs 29, 30, and 36), the same simulations can be used to show that just a few discrete hydrogen-bonding structures coexist in water, and that these structures can give rise to structurally distinguishable subbands. Quite recently, two groups have made important advances in simulations of HOD/D_2O allowing them to investigate ν_{OH} dynamics including spectral diffusion and VR pathways and lifetimes.[29−31,36−42] However, these simulations have been used to extract only ensemble-averaged dynamics, so the issue of dynamically distinguishable subbands has not yet been dealt with.

These issues raised by experiments and simulations are sometimes termed the continuous environment versus multicomponent controversy.[31,36] The experimental methods used in this work are well suited to help resolve this issue. The anti-Stokes Raman probe technique allows us to simultaneously monitor both the *decay of the parent* ν_{OH} excitation and the *appearance of the daughter* bend δ_{H_2O} in water and the δ_{HOD} or δ_{D_2O} daughters in HOD/D_2O as a function of both pump and probe frequency within the ν_{OH} band.[27] Thus we can investigate the question of dynamically distinguishable subbands by direct measurements of both the VR lifetime and the VR pathway. Here we advocate the multicomponent (actually two-component) picture as a result of our observations of both water and HOD/D_2O.

A. Spectroscopy of Water and HOD/D_2O. The stretching bands of water and HOD/D_2O are inhomogeneously broadened. The large (fwhm 350−450 cm^{-1}) spectral widths reflect an underlying broad distribution of hydrogen-bonding parameters. The IR and Raman spectra of water are shown in Figure 1. In water, the stretching transition (∼2900−3700 cm^{-1}) is complicated by the coexistence of three overlapping transitions: the symmetric and antisymmetric stretch and the bending overtone $2\delta_{H_2O}$. In Figure 1a, we used an admittedly crude method[22] for illustrating the contribution of $2\delta_{H_2O}$ in the ν_{OH} region. The measured IR absorption spectrum of the bend fundamental ($v = 0 \rightarrow 1$) transition $I_\delta(\nu)$, centered near 1640 cm^{-1}, was used to construct a function representing the overtone transition ($v = 0 \rightarrow 2$), $I_\delta(2\nu-\nu')$, where $\nu' \approx 40$ cm^{-1} is the gas-phase anharmonicity.[43] This putative overtone transition in Figure 1a is concentrated primarily in the lower frequency part of the ν_{OH} transition. The IR and Raman stretch spectra of water and its isotopomers are frequently fit with a small number of overlapping Gaussian subbands.[2] The Raman spectrum of water in Figure 1 clearly evidences a dual-peak structure (3235 and 3460 cm^{-1}). A pair of Gaussian subbands does a good job of fitting the Raman spectrum, although a better fit is accomplished by using one additional minor subband at the red edge and one at the blue edge.[2,22]

The HOD in D_2O system (HOD/D_2O) may be viewed as simpler than water because, as shown in Figure 2, there is little overlap between the ν_{OH}, $2\delta_{HOD}$, and ν_{OD} transitions. The putative bend overtone spectrum in Figure 2 (the fundamental δ_{HOD} is peaked at 1443 cm^{-1}) lies primarily though not entirely outside the ν_{OH} band. The Raman spectrum of HOD in Figure 2 has a less-prominent dual-peak structure, with a main subband peaked near 3422 cm^{-1} and a second smaller and narrower peak on the blue edge near 3590 cm^{-1}.

B. Structural Environments and Stretching Transitions. In water, the red shift within the ν_{OH} transition (relative to a solitary[44] water molecule) is generally associated with stronger hydrogen bonding.[2] Studies of water in a series of hydrogen-bonded solids led to the suggestion of a possible 1:1 correspondence between the ν_{OH} wavenumber and the hydrogen bond length.[45,46] This suggestion was subsequently employed to simplify the interpretation of ultrafast nonlinear spectroscopy measurements[14,16,47] of HOD/D_2O. Using pump and probe pulses that were spectrally narrower than the ν_{OH} band would make it possible to study water molecules having similar hydrogen bond lengths. For instance, molecules with instantaneously longer hydrogen bonds could be pumped and the subsequent evolution toward shorter hydrogen bonds could be probed.[14,16] However, recent simulations have shown the matter is not so simple.[30,31,36] It turns out there is a considerable dispersion of energies for molecules with a particular hydrogen bond length or strength, so such a simple structural interpretation of nonlinear spectroscopy is not possible.

Simulations are excellent tools for examining the underlying structures of liquid water. However, determining whether hydrogen bonds exist between adjacent molecules presents a problem and usually relies on potentially arbitrary energetic or geometric criteria. With geometric criteria, a pair of molecules

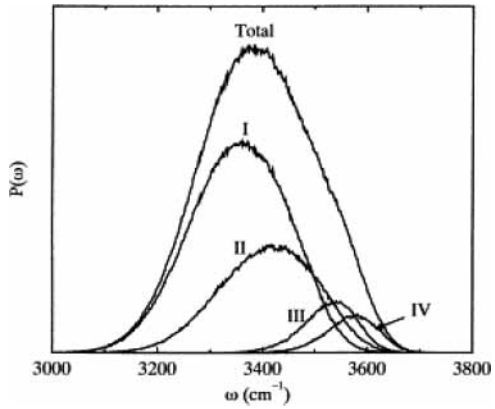

Figure 3. Computed density of states for four hydrogen-bonded configurations of HOD/D_2O, reprinted with permission of the copyright holder, Elsevier, from ref 29. Region I consists mostly of "ice-like" molecules with approximately four hydrogen bonds, and the other regions represent molecules with one or two broken bonds.

are hydrogen bonded if the distance is shorter than a critical value and the angle is smaller than a critical value. In Figure 3, reproduced from a recent paper by Lawrence and Skinner,[29] geometric criteria were applied to a simulation of HOD/D_2O to detail the structures underlying the ν_{OH} transition. The overlapping subbands denoted I−IV represent the four possibilities where the H-atom has either zero or one or more hydrogen bonds and where the O-atom has either one or two or more hydrogen bonds. Since the D-atom may have zero or one or more hydrogen bonds as well, subband I corresponds *for the most part* to "ice-like" HOD with approximately four hydrogen bonds, the subbands II and III correspond for the most part to HOD with three hydrogen bonds, and the subband IV corresponds for the most part to HOD with two hydrogen bonds.[29]

C. Ultrafast Pump−Probe Measurements. Several groups have used one-color and two-color mid-IR pump−probe techniques to study ν_{OH} of HOD/D_2O. Since comprehensive reviews of these studies have recently appeared,[31,42,48] here we will discuss only results deemed germane to the multicomponent versus continuous environment problem.

In 1997, Woutersen et al.[12] used one-color and two-color mid-IR pump−probe techniques with HOD/D_2O to study orientational relaxation within ν_{OH} via the polarization anisotropy decay. The anisotropy decay became slower on the red edge, which agreed with the notion that stronger hydrogen-bonded environments led to slower orientational relaxation. These authors went on to assert that the orientational relaxation lifetime did not vary smoothly across ν_{OH} but rather had two distinct values, $\tau_{or} = 0.7$ ps and $\tau_{or} = 13$ ps, which was taken as evidence for a "two-component" structure. The slowly rotating component was suggested to arise from molecules that must break a hydrogen bond in order to rotate.[12] The water VR lifetime of $T_1 = 0.7$ ps was said to *increase* slightly moving to the blue. In subsequent work by the same group[11] where one-color and two-color methods were found to give different lifetimes, the lifetime was said to *decrease* slightly moving to the blue.

At about the same time, Laenen et al. used two-color mid-IR pump−probe techniques to obtain transient spectra[3,4] of ν_{OH} in HOD/D_2O between 275 and 345 K. The spectra were interpreted with use of three Gaussian subbands. On the basis of Rahman and Stillinger's water simulations,[32] the subbands were assigned to different water structures. At ambient temperature, subband I peaked near 3340 cm^{-1} with fwhm = 40 cm^{-1} and $\tau_{or} = 10$ ps was attributed to tetrahedral "ice-like" water. Subband II peaked near 3400 cm^{-1} with fwhm 60 cm^{-1} and $\tau_{or} = 13$ ps was attributed to water with "bridged" hydrogen bonds. Subband III peaked near 3440 cm^{-1} with fwhm = 140 cm^{-1} and $\tau_{or} = 3$ ps was attributed to water with "bifurcated" hydrogen bonds. Some less significant subbands were also invoked to explain the temperature dependence and effects of $2\delta_{HOD}$. The ν_{OH} VR lifetime near the band center was given as $T_1 = 1.0$ ps.

In 1999, Gale et al. used two-color mid-IR pump−probe methods[18] to measure the VR lifetime of ν_{OH} in HOD/D_2O. Their data were interpreted in terms of a VR lifetime that increased with blue shift, from 0.47 ps at 3270 cm^{-1} to 0.97 ps at 3600 cm^{-1}.

In our experiments,[22,23,26−28,49,50] a mid-IR pump pulse is combined with an incoherent anti-Stokes Raman probe (IR−Raman technique, a type of 3D vibrational spectroscopy[51]). The pump pulse is tuned to generate $\upsilon = 1$ excitations of the parent vibration ν_{OH}. Using a multichannel spectrograph, we simultaneously monitor the anti-Stokes spectrum over a wide range (here 500−4000 cm^{-1}) that includes all stretching and bending transitions. The anti-Stokes signal is sensitive only to excited states,[1] including the parent ν_{OH} plus whatever daughters are created by parent decay.[22,27] The anti-Stokes signal is proportional to the instantaneous occupation number multiplied by the Raman cross-section,[1,52] which is approximately given by the Stokes Raman spectra in Figures 1b and 2b. In water, the anti-Stokes signals in the stretching region (∼2800−3700 cm^{-1}) arise only from the parent ν_{OH} excitation via the $\upsilon = 1 \rightarrow 0$ transition. In the bending region (∼1640 cm^{-1}) the signals arise from δ_{H_2O} daughter excitations created by parent decay, via either the $\upsilon = 2 \rightarrow 1$ overtone transition[26,52,53] or the $\upsilon = 1 \rightarrow 0$ fundamental transition. In HOD/D_2O experiments, signals in the ν_{OH} region (∼2800−3700 cm^{-1}) originate from the parent via the $\upsilon = 1 \rightarrow 0$ transition.[26] Signals in the ν_{OD} region (∼2000−2600 cm^{-1}) result from ν_{OD} daughters of both HOD and D_2O, observed via the $\upsilon = 1 \rightarrow 0$ transitions. The signals in the δ_{HOD} (∼1440 cm^{-1}) and δ_{D_2O} regions (∼1220 cm^{-1}) also arise from daughters, observed via the fundamental or the overtone transitions.[26]

Differences between the mid-IR probe and anti-Stokes Raman techniques have been discussed previously.[1,26,50,51,54] Whereas anti-Stokes probing sees only excited states, IR probes simultaneously see pump-induced transmission changes due to ground-state depletion, excited-state induced emission, and excited-state absorption. Understanding the complicated pattern of bleaching and transient absorption effects that results[19] requires a good deal of modeling[14,55] to incorporate the simultaneous effects of dynamics occurring in the $\upsilon = 0$, 1, and 2 states of the parent ν_{OH} and in excited states of daughters generated by ν_{OH} decay. Unfortunately these models require a detailed knowledge of absorption cross-sections that have not yet been well characterized, for transitions among several excited states.[26,54]

In 2000, Deàk et al. used the IR−Raman technique[22] to study both water and HOD/D_2O. They observed the generation of δ_{H_2O} daughters from ν_{OH} decay in water and the generation of ν_{OD}, δ_{HOD}, and δ_{D_2O} daughters from ν_{OH} decay of HOD. VR of both isotopomers was observed to be faster on the red edge than on the blue edge of ν_{OH}. In 2003, our group used an improved laser apparatus to reexamine water.[26−28] It was found that ν_{OH} dynamics of water could be explained by using two inhomogeneously broadened Gaussian subbands.[27,28] The dominant subband was a broader (fwhm ∼ 400 cm^{-1}) red-shifted band with a peak near 3250 cm^{-1} that had $T_1 = 0.55$ ps. Decay of this red-shifted band occurred via two parallel VR pathways,[27]

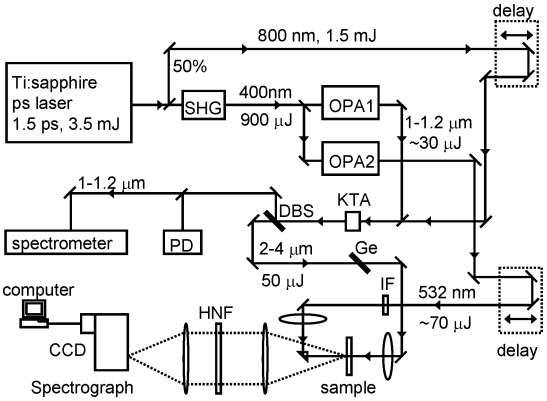

Figure 4. Block diagram of the laser system. Key: SHG = second-harmonic generator; OPA = optical parametric amplifier; KTA = potassium titanyl arsenate mixer crystal for mid-IR generation; DBS = dichroic beam splitter; PD = photodiode; Ge = germanium Brewster window; IF = 25 cm^{-1} fwhm interference filter at 532 nm; HNF = holographic notch filter, CCD = charge-coupled device optical detector. OPA1 is tuned from 1.0 to 1.176 μm to produce IR in the 2500−4000-cm^{-1} range, and OPA2 is fixed at 532 nm.

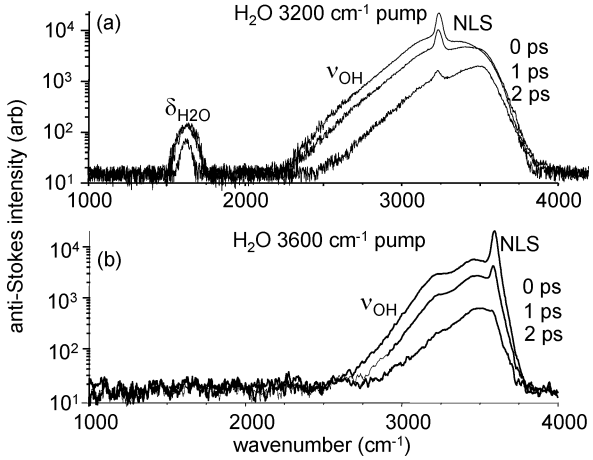

Figure 5. Transient anti-Stokes spectrum of water with red-edge pumping at 3200 cm^{-1} and blue-edge pumping at 3600 cm^{-1}. The narrower peak at the pump wavenumber is a coherence artifact due to nonlinear light scattering (NLS). Decay of the parent ν_{OH} excitation produces δ_{H_2O} daughter excitations with red-edge pumping but not with blue-edge pumping.

$\nu_{OH} \rightarrow \delta_{H_2O}$ (1/3) and $\nu_{OH} \rightarrow$ ground state (2/3). The blue-shifted subband peaked near 3500 cm^{-1} was narrower (fwhm ~ 200 cm^{-1}) and longer lived, having a 0.75-ps lifetime. Decay of this blue-shifted subband generated[27] no detectable δ_{H_2O}, so it was presumed to occur entirely by the $\nu_{OH} \rightarrow$ ground-state pathway. Following the nomenclature of those works, we will henceforth term the red-shifted and blue-shifted components of the ν_{OH} band ν_{OH}^{R} and ν_{OH}^{B}.

In previous work,[28] we presented data indicating that ν_{OH} dynamics of water could be explained using two dynamically distinguishable vibrational subbands. In the present work we present data on HOD/D_2O along with additional data on water to facilitate comparisons between these isotopomers. We will show that both water and HOD/D_2O are equally well described with two inhomogeneously broadened subbands, and that a comparison of water and HOD allows us to clarify the origin of these two subbands.

2. Experimental Section

The IR−Raman experimental apparatus has been described previously,[49,56] but we now use an improved laser system. A block diagram of the 1-kHz laser is shown in Figure 4. A tunable mid-IR pulse (25 cm^{-1} bandwidth, 370 μm diameter, ~0.7 ps, variable energy <50 μJ) pumps a free-flowing jet of water. A 532-nm visible Raman probe pulse (15 cm^{-1} bandwidth, 400 μm diameter, ~0.7 ps, typically 25 μJ) generates an anti-Stokes spectrum detected by a multichannel spectrograph.[22] The coherent sum-frequency from the surface at $\omega_{IR} + \omega_{vis}$ is blocked by slightly tilting the jet. The remaining sum-frequency signal from the bulk,[57−59] sometimes termed nonlinear light scattering (NLS), cannot be eliminated resulting in a coherent artifact. In our anti-Stokes spectra, this artifact appears at the same wavenumber as the pump pulse. The time dependence of this NLS artifact is used to characterize the laser time and frequency response.[26]

Of particular concern in water experiments is the large ν_{OH} absorption coefficient that, combined with intense pump pulses, can lead to a large excitation density.[24−28,54,60] Effects associated with high-density excitations are characterized by the temperature jump ΔT that results after several picoseconds, when VR is complete. The value of $\Delta T = J\alpha/C$ is determined from J the IR fluence, α the absorption coefficient, and C the heat capacity.[26,54] In ΔT-dependent studies, we have determined that the VR lifetimes and pathways are minimally affected by ΔT as long as ΔT is kept below[26,54] 30 K. In water experiments, measurements with mid-band pumping were kept below ΔT = 30 K, and measurements with band-edge pumping had even smaller ΔT. The HOD/D_2O measurements use a diluted solution of OH absorbers, so that even with midband pumping ΔT never exceeds 8 K. Due to the relative insensitivity of Raman scattering, our HOD/D_2O samples are more concentrated[22] (10% HOD in D_2O) than those used by other labs. However, we do not believe this presents any problem. The most significant absorbing impurity in the ν_{OH} region is H_2O; it is only 10% of the HOD concentration.[22] We obtain excellent agreement with the accepted[13,18,38] ν_{OH} lifetime of ~0.9 ps. At this concentration, the possibility of intermolecular vibrational energy transfer between OH groups is known to be small, based on the concentration dependence of the polarization anisotropy decay.[15]

3. Results

A. Transient Raman Spectra. Figure 5 shows transient Raman spectra of water pumped near the red and blue edges of the ν_{OH} absorption, at 3200 and 3600 cm^{-1}. Recall that the signal intensity is proportional to the number of excited states and the Raman cross-section. With red-edge pumping the decay is faster on the red edge; with blue-edge pumping the decay is similar throughout the band. Below we will explain this as a consequence of having a shorter-lived red-shifted subband, a longer-lived blue-shifted subband, and slow interconversion. Parts a and b in Figure 5 indicate that red-edge and blue-edge pumping of ν_{OH} lead to different VR pathways. Red-edge pumping produces δ_{H_2O} daughters while blue-edge pumping does not. The ratio of ν_{OH} to δ_{H_2O} intensities can be used to determine the absolute quantum yield for the $\nu_{OH} \rightarrow \delta_{H_2O}$ pathway.[22,27] The ν_{OH} Raman cross-section is about 50 times bigger than the δ_{H_2O} cross-section[27] (see Figure 1b). The quantum yield for $\nu_{OH} \rightarrow \delta_{H_2O}$ with red-edge pumping is found to be ~1/3; with blue-edge pumping it is ~0. Since ν_{OH} of water has only two possible VR pathways, $\nu_{OH} \rightarrow \delta_{H_2O}$ or $\nu_{OH} \rightarrow$ ground state, the VR pathways of ν_{OH} of water can be summarized as $\nu_{OH} \rightarrow \delta_{H_2O}$ (1/3) and $\nu_{OH} \rightarrow$ ground state (2/3) for red-edge pumping and $\nu_{OH} \rightarrow$ ground state for blue-edge pumping.[27]

Figure 6 shows transient anti-Stokes Raman spectra for HOD/D_2O with 3180-cm^{-1} red-edge and 3550-cm^{-1} blue-edge

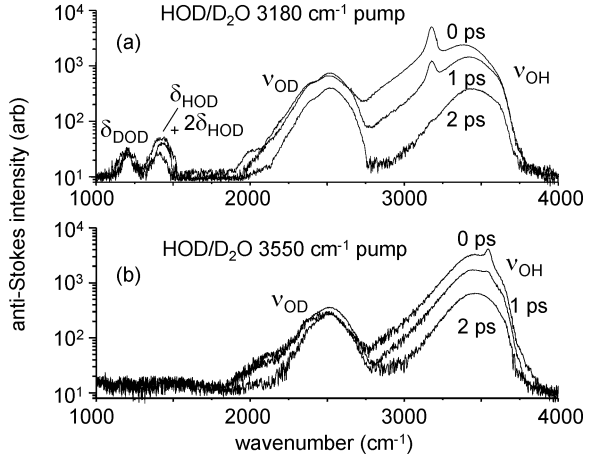

Figure 6. Transient anti-Stokes spectrum of HOD/D_2O with red-edge pumping at 3180 cm^{-1} and blue-edge pumping at 3550 cm^{-1}. The narrow peak at the pump wavenumber is a coherence artifact. Decay of the parent ν_{OH} excitation with blue-edge pumping produces ν_{OD} daughter excitations. Parent decay with red-edge pumping produces more ν_{OD} plus δ_{HOD} and δ_{D_2O}.

pumping. As with water, with red-edge pumping the decay rate is faster on the red edge, while with blue-edge pumping the decay rate is similar across the band, and the ν_{OH} decay pathways are dependent on pump frequency. With blue-edge pumping, the only observed daughter is ν_{OD}. With red-edge pumping we observe more ν_{OD} plus δ_{HOD} and δ_{D_2O}. Notice that there is no detectable signal from water δ_{H_2O}, which indicates that the H_2O impurity is not contributing significantly to these signals. This is not because the rate of δ_{H_2O} disappearance is especially fast in HOD/D_2O solutions, since with somewhat greater H_2O concentrations we do see δ_{H_2O} alongside δ_{HOD} and δ_{D_2O}.

Understanding the detailed relaxation pathways of ν_{OH} in HOD/D_2O, especially what fraction of the observed bending excitations should be attributed to the bend fundamentals or bend overtones, is of great current interest.[31,36−38,41,42] For the present simply note that there is a significant dependence of the VR pathway on the pump wavenumber, which had not been observed or proposed previously. More detailed studies of these pathways will be forthcoming. These studies will show that in HOD/D_2O, the first-generation daughters of ν_{OH} include ν_{OD} and both $2\delta_{HOD}$ and δ_{HOD} (notice how the δ_{HOD} line shape changes with time in Figure 6a). The δ_{D_2O} seen in Figure 6a is not a first-generation daughter of ν_{OH}, because the rise of δ_{D_2O} is slower than the fall of ν_{OH}. Instead, δ_{D_2O} is a second-generation daughter generated primarily by the $\nu_{OH} \rightarrow \nu_{OD} \rightarrow \delta_{D_2O}$ pathway.

B. Decomposition into Gaussian Subbands. Our decomposition of ν_{OH} excited-state spectra into Gaussian subbands[23,28] is illustrated in Figures 7−11. The water data at all delay times and pump frequencies could be fit by using two Gaussian subbands, termed ν_{OH}^{R} and ν_{OH}^{B}, plus a much narrower Gaussian to represent the NLS artifact. Additional water data of this type at other pump frequencies can be seen in Figures 1 and 2 of ref 28. For the HOD/D_2O data in Figure 9, we also used just two Gaussian subbands plus one Gaussian for the NLS artifact. However, with higher frequency pumping in HOD/D_2O we found it necessary to include a minor subband on the blue edge, as shown in Figures 10 and 11. For completeness, in our analysis of Figures 9−11 we also fit the ν_{OD} spectral region[23] where there is a mixture of excited-state D_2O and HOD, using either one or two Gaussians. But whatever method we used to fit the ν_{OD} region had no effect on our analysis of the ν_{OH} region.

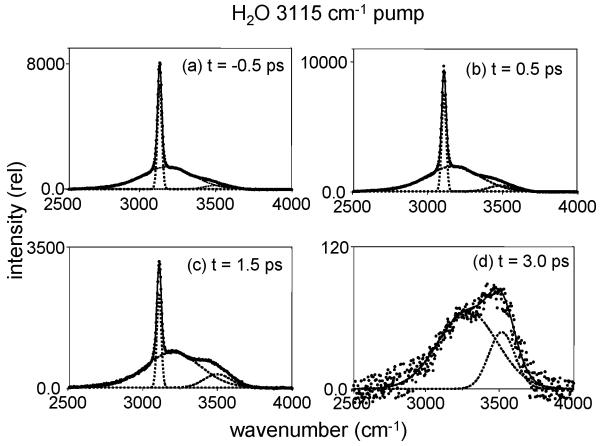

Figure 7. Transient anti-Stokes spectra in the ν_{OH} region of water with red-edge 3115-cm^{-1} pumping. The spectra were fit by using a broader red-shifted Gaussian subband termed ν_{OH}^{R} and a narrower blue-shifted Gaussian subband termed ν_{OH}^{B}, along with a much narrower Gaussian function to represent the coherence artifact. In water, ν_{OH}^{R} is the major subband and ν_{OH}^{B} the minor subband.

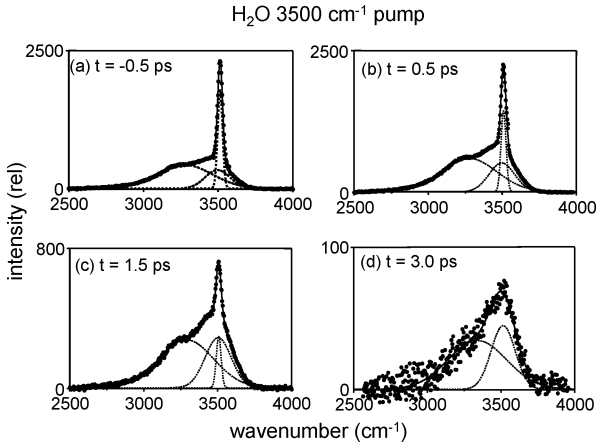

Figure 8. Transient anti-Stokes spectra in the ν_{OH} region of water with blue-edge 3500-cm^{-1} pumping. The spectra were fit by using two Gaussian subbands ν_{OH}^{R} and ν_{OH}^{B}, as in Figure 7.

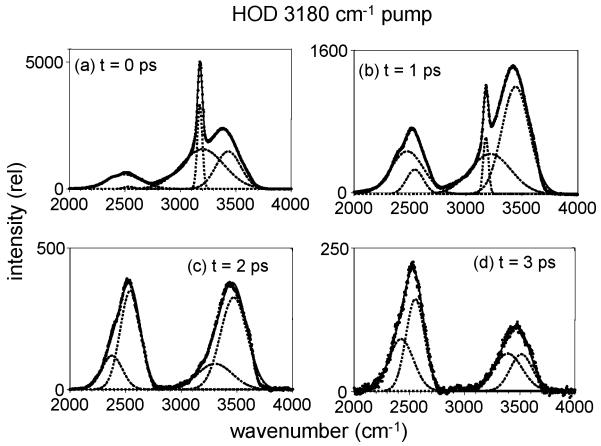

Figure 9. Transient anti-Stokes spectra in the ν_{OH} region of HOD/D_2O with red-edge 3180-cm^{-1} pumping. The spectra were fit by using two Gaussian subbands ν_{OH}^{R} and ν_{OH}^{B}, as in Figure 7. In HOD/D_2O, ν_{OH}^{B} is the major subband.

C. Time Dependence of Subband Peaks, Widths, and Amplitudes. The peaks and fwhm of the two major subbands ν_{OH}^{R} and ν_{OH}^{B} of water[28] and HOD/D_2O vary with time and with pump wavenumber, as shown in Figure 12. Figure 12 shows

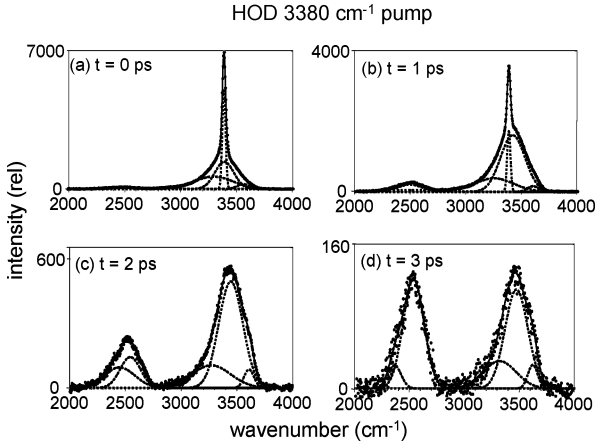

Figure 10. Transient anti-Stokes spectra in the ν_{OH} region of HOD/D_2O with midband 3380-cm^{-1} pumping. To fit the blue edge, a minor subband peaked at 3650 cm^{-1} was added. This minor subband evidenced the same dynamical behavior as ν_{OH}^{B}.

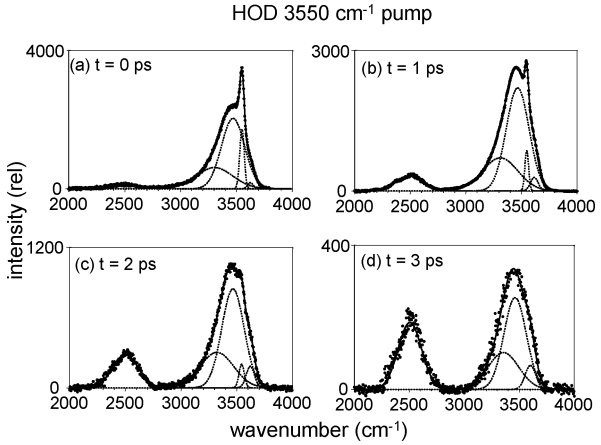

Figure 11. Transient anti-Stokes spectra in the ν_{OH} region of HOD/D_2O with blue-edge 3550-cm^{-1} pumping, fit by using ν_{OH}^{R} and ν_{OH}^{B} subbands along with a minor subband peaked at 3650 cm^{-1}.

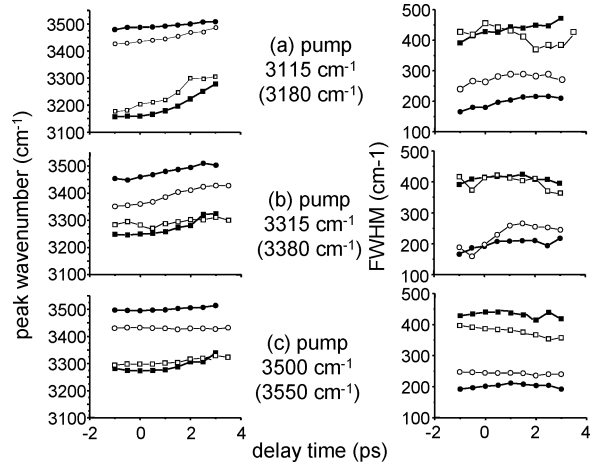

Figure 12. Time dependence of the peak locations and fwhm of the ν_{OH}^{R} (squares) and ν_{OH}^{B} (circles) subbands of water (filled symbols) and HOD/D_2O (open symbols) pumped on the ν_{OH} red edge, the blue edge, and in the middle of the band (the HOD pump wavenumbers are in parentheses). The ν_{OH}^{R} subband evidences similar behavior in water and HOD/D_2O. Compared to water, in HOD/D_2O the ν_{OH}^{B} subband is broader and red shifted.

that the behavior of ν_{OH}^{R} is similar in water and HOD/D_2O, whereas ν_{OH}^{B} in HOD/D_2O is red shifted by ~100 cm^{-1} and is ~50% broader than in water. The initial peak locations (near t = 0) of both subbands can be shifted somewhat by tuning the pump frequency. Generally speaking, red-shifted pump pulses pull the initial peak locations farther to the red than blue-shifted pulses pull the peaks to the blue, and the initial peak location of ν_{OH}^{R} is more sensitive to pump frequency than ν_{OH}^{B}. As time progresses, the subbands typically undergo a blue shift, although the blue shift is minimal with higher frequency pump pulses. Regardless of the initial location, it appears as if each subband peak in each isotopomer tends toward a particular destination at longer delay. The longer time destinations of the subband peaks are 3325 and 3525 cm^{-1} for ν_{OH}^{R} and ν_{OH}^{B} of water and 3310 and 3455 cm^{-1} for ν_{OH}^{R} and ν_{OH}^{B} of HOD. The minor subband on the blue edge of the HOD spectrum never moved much from a peak location of 3650 cm^{-1}. We view this motion toward a single destination for each subband regardless of pump frequency as suggestive that the cited destinations represent the equilibrium locations of the subband peaks (within an estimated error of ±25 cm^{-1}), with the caveat that due to excited-state decay we cannot accurately measure beyond delays of ~4 ps.

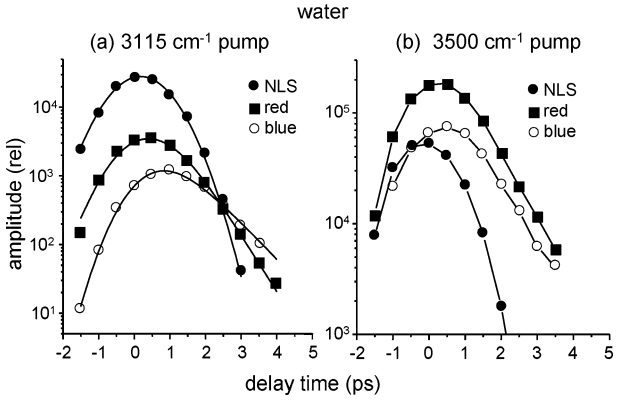

Figure 13. Time dependence of the subband amplitudes in water. NLS denotes the nonlinear light-scattering coherence artifact that gives the apparatus time response. (a) With red-edge pumping the ν_{OH}^{R} (red) subband builds up instantaneously and the ν_{OH}^{B} (blue) subband has a delayed buildup. (b) With blue-edge pumping both subbands build up instantaneously, and at longer delay times both subbands decay with the (longer) ν_{OH}^{B} lifetime. The ν_{OH}^{R} subband is dominant in water.

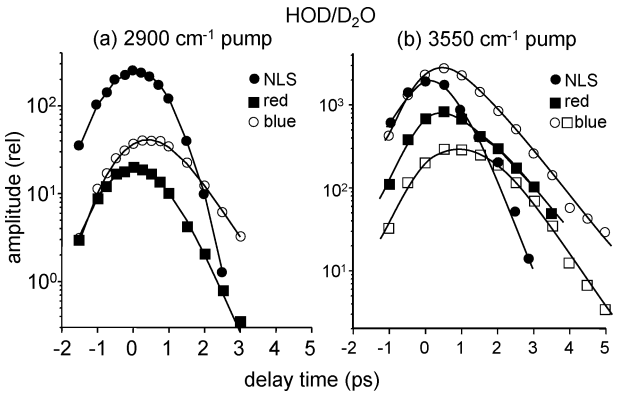

Figure 14. Time dependence of the subband amplitudes in HOD/D_2O. NLS denotes the nonlinear light-scattering coherence artifact that gives the apparatus time response. (a) With both red-edge and blue-edge pumping, the ν_{OH}^{B} (blue) subband is dominant in HOD. (b) With blue-edge pumping, a minor subband peaked near 3650 cm^{-1} (open squares) is added to fit the spectrum. However, the time dependence of this third subband is indistinguishable from the ν_{OH}^{B} subband.

The time dependences of the subband amplitudes are shown in Figures 13 and 14. Under almost all conditions, in water[28] the ν_{OH}^{R} subband was dominant (had the greater area) whereas ν_{OH}^{B} was dominant in HOD/D_2O. With red-edge pumping, ν_{OH}^{R}

builds up instantaneously (as determined by the NLS artifact) but ν_{OH}^{B} has a delayed buildup.[28] The delayed buildup of ν_{OH}^{B} occurs with a time constant that is within experimental error equal to the ν_{OH}^{R} lifetime. The ν_{OH}^{R} lifetime is 0.55 ps in water and 0.48 ps in HOD, with an estimated error of ±0.05 ps. The ν_{OH}^{B} lifetime is 0.75 ps in water and 0.73 ps in HOD, with an estimated error of ±0.08 ps. With blue-edge pumping in water, both ν_{OH}^{R} and ν_{OH}^{B} subbands appear to build up instantaneously, and they both decay with similar ~0.75-ps lifetimes. With blue-edge pumping in HOD, both major subbands build up instantaneously: ν_{OH}^{B} decays with a 0.9-ps lifetime and ν_{OH}^{R} decays with a slightly shorter 0.8-ps lifetime.

We tried to determine whether the minor subband in HOD near 3650 cm^{-1} could be dynamically distinguished from the major ν_{OH}^{B} subband. In an effort to pump only this minor subband, we made measurements with the pump laser tuned to 3680 cm^{-1}. We found that within experimental error, both the minor subband and ν_{OH}^{B} always evidence the same buildup and decay kinetics and similar amplitude ratios, which leads us to believe that these two subbands are dynamically indistinguishable. Therefore with the data we have obtained, there is no compelling reason to believe there are more than two distinct subbands in HOD/D_2O, and henceforth when we refer to ν_{OH}^{B} of HOD/D_2O we mean that the ν_{OH}^{B} subband has a dual-Gaussian shape consisting of a larger broader peak with a much smaller (~12% area) narrower peak on its blue edge.

D. Fixed-Wavenumber Transients. Most of the IR probe studies mentioned earlier use a method of data acquisition and analysis that we term[28] "fixed-wavenumber transients". In this method the probe wavenumber is fixed and the time delay scanned. Note our data in Figures 13 and 14 are not single-wavenumber transients, but rather time-dependent amplitudes of subbands that undergo spectral diffusion. For the sake of comparison to other works, we converted our data to the single-wavenumber format. In general, a fixed-wavenumber transient reflects[3,4,18] *the combined effects of spectral diffusion and VR*. With our anti-Stokes Raman probing method, a fixed-wavenumber transient in the ν_{OH} region is a signal that is always positive, which is sensitive to excited-state spectral diffusion and excited-state population decay. In mid-IR experiments, fixed-wavenumber transients usually evidence a complicated and nonmonotonic pattern of positive and negative-going amplitudes[19] reflecting the simultaneous contributions of spectral diffusion and population relaxation in the ν_{OH} ground and excited states and in daughter excitations[26,54] such as δ_{H_2O}.

Our fixed-wavenumber transients were fit by convolving the apparatus response with a single-exponential decay. These *effective exponential decay constants* at different probe wavenumbers (10-cm^{-1} window) are plotted in Figure 15 for water and HOD with red-edge pumping. A fixed-wavenumber probe near the red edge sees the fastest decay constant, which results from a combination of the 0.5-ps ν_{OH}^{R} lifetime and the ν_{OH}^{R} blue shift. This blue shift reduces the decay constant below 0.5 ps, with the amount of reduction dependent on the slope of the ν_{OH}^{R} subband at the probe wavenumber. The effective decay constants level off at values around 0.35 ps near the red edge. These values are at best an estimate,[26−28,54] given our 0.7 ps pulse duration, and may well be even smaller. A fixed-wavenumber probe near the blue edge sees the ~0.8-ps ν_{OH}^{B} lifetime, plus an additional gradual rise in signal due to the time-dependent blue shift of both ν_{OH}^{R} and ν_{OH}^{B}. However, the effect of spectral diffusion here is not great, resulting in only a slight increase of ~10% over the ν_{OH}^{B} lifetime.

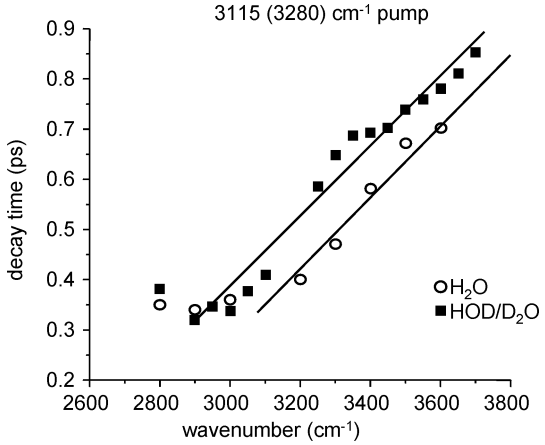

Figure 15. Anti-Stokes data with red-edge pumping (for water 3115 cm^{-1} and for HOD/D_2O 3280 cm^{-1}) analyzed by the single-wavenumber transient method. The effective exponential decay time constant at each probe wavenumber interval (10 cm^{-1}) reflects contributions from both spectral diffusion and population relaxation, and it evidences a continuous increase moving from red to blue.

Our Raman data for HOD in the fixed-wavenumber format appear to agree well with work from three other laboratories, who all observe a lifetime of ~0.9 ps for the main part (our ν_{OH}^{B}) of the ν_{OH} transition.[13,18,38] In addition, the effective decay time constants for HOD in Figure 14 are in excellent agreement with those of Gale et al., who observed[18] relaxation times ranging from 0.5 ps at 3270 cm^{-1} to 1.0 ps at 3600 cm^{-1}. The only comparison possible for water is with data from Lock and Bakker,[24,25,60] and here we have considerable disagreement. Those authors interpreted their mid-IR transients[24,25,60] as indicating a ν_{OH} decay of 0.26 ps to an intermediate state, followed by a ground-state recovery of 0.55 ps. This disagreement was debated recently.[54,60] It is our position that both mid-IR and Raman probe experiments measure the same effects but that the mid-IR transient data have been interpreted incorrectly.[26,54] Our data in Figures 5 and 15 clearly demonstrate that the water VR lifetime is much longer than 0.26 ps. Lock and Bakker[24,25] explained their data by postulating an intermediate state with a 0.55-ps lifetime. However, we have made direct measurements of an intermediate state, δ_{H_2O}, which turns out to have a 1.4-ps lifetime.[27,54] We associate their 0.26-ps time constant with the 0.35-ps time constant in Figure 15 that arises from spectral diffusion plus population relaxation (our 0.35-ps value presumably results from our longer pulse duration) and the 0.55-ps time constant with our 0.55-ps value for the lifetime of the dominant ν_{OH}^{R} subband.

4. Discussion

A. Continuous versus Two-Component Environments. Figure 15 is suggestive that ν_{OH} of water or HOD/D_2O can be described by a frequency-dependent lifetime that increases continuously from red to blue. This is the view espoused by several authors.[11,12,18] On the other hand, Figures 7−12 are suggestive of water and HOD/D_2O having just two major coexisting and interconverting subbands with different lifetimes. The key observation that decides between these views is our discovery that the subbands denote regions of distinctively different VR pathways. In this paper we have shown in Figures 5 and 6 that pumping either subband results in parent decay leading to different daughter vibrations. An additional and significant piece of evidence is given in Figure 2d of ref 27. In water, ν_{OH}^{R} generates δ_{H_2O} daughters whereas ν_{OH}^{B} does not, and

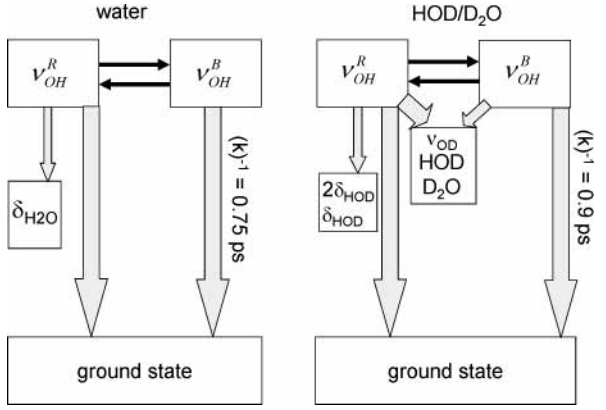

Figure 16. Schematic of vibrational relaxation (VR) pathways for both subbands of ν_{OH} in water and in HOD/D_2O. The width of each arrow is approximately proportional to the rate. Both ν_{OH}^R and ν_{OH}^B decay to the ground state with similar rates, but ν_{OH}^R has an additional decay channel involving the bending vibration that results in a shorter lifetime. Interconversion between subbands is slower than any observed decay pathway.

this plot shows that the frequency-dependent quantum yield for $\nu_{OH} \rightarrow \delta_{H_2O}$ generation quite closely tracks the ν_{OH}^R spectrum.

The VR pathways of the two subbands in water and HOD/D_2O are illustrated in Figure 16. In the figure, the relative rates of each pathway are depicted by the widths of the arrows. Figure 16 is a reminder that the rates of the $\nu_{OH}^R \rightarrow$ ground state and $\nu_{OH}^B \rightarrow$ ground-state processes are quite similar and that the shorter lifetime of ν_{OH}^R is due to its having an additional VR pathway to δ_{H_2O}. In addition, in HOD/D_2O the $\nu_{OH}^R \rightarrow \nu_{OD}$ pathway is faster than the $\nu_{OH}^B \rightarrow \nu_{OD}$ pathway. As explained above, we did not diagram a $\nu_{OH} \rightarrow \delta_{D_2O}$ decay pathway in Figure 16 for HOD/D_2O, because δ_{D_2O} is a *second-generation daughter* produced by the $\nu_{OH} \rightarrow \nu_{OD} \rightarrow \delta_{D_2O}$ process.

The ν_{OH}^R subband amplitude in HOD/D_2O is always quite a bit smaller than that in water, but the ν_{OH}^R lifetime, peak location, peak shift, and fwhm are quite similar in both. For this reason, we were concerned that the ν_{OH}^R subband seen in HOD/D_2O might actually result from the H_2O impurity in the HOD/D_2O sample, where H_2O is about 10% of the HOD concentration. However, we could rule out this possibility because ν_{OH}^R subband decay in water generates δ_{H_2O} whereas ν_{OH}^R subband decay in HOD/D_2O does not.

Although both subbands are inhomogeneously broadened, the VR lifetime is apparently constant throughout each subband. Some of the time-dependent changes in peak location and fwhm seen in Figure 12 might be due to a frequency-dependent lifetime, but if the lifetime had a significant frequency dependence, the subbands would have a non-Gaussian shape at longer time that is not observed. Thus the distribution of ν_{OH} VR lifetimes in water and in HOD/D_2O is seen to be approximately bimodal, having at most only a narrow spread around the two distinct values 0.55 ps (0.48 ps) and 0.75 ps (0.9 ps), where values in parentheses refer to HOD/D_2O. The ν_{OH}^R and ν_{OH}^B subbands are spectroscopically contiguous regions of the ν_{OH} band, within which $v = 1$ excitations have approximately identical VR lifetimes and decay pathways.

The existence of these two distinctive subbands was not seen in the mid-IR probe studies cited earlier, with either water or HOD/D_2O, for several reasons. We have the ability to distinguish subband dynamics by monitoring the pump-frequency dependent generation of daughter vibrational excitations, which has not yet been possible with IR methods. With anti-Stokes Raman probing we do not have to rely on models to disentangle the combined effects of intermediate states and excited state absorptions. Since our Raman spectra need minimal data processing, and since we simultaneously acquire the signal across a wide spectral region of 1000−4000 cm^{-1}, our spectra have a better signal-to-noise ratio than transient spectra obtained previously.

B. Interconversion between Subbands. Our data indicate that subbands interconvert on a time scale of a few picoseconds. However, it is difficult for us to measure interconversion rates with high accuracy. The difficulty stems from not knowing how much of each subband is excited by a particular mid-IR pump frequency and the problem of disentangling the subband shifting, broadening ,and VR processes from subband interconversion. Generally speaking, if the subbands interconverted faster than about 1 ps, we would not see distinctly different subband lifetimes. If the subbands interconverted slower than several picoseconds, results seen in Figures 7 and 9 would be unlikely. These figures show that with red-edge pumping that excites only ν_{OH}^R, the two subband amplitudes approximately equalize at the longest delay times where measurements remain reasonably accurate, about 3 ps. A quantitative analysis can be made in the case of water with red-edge pumping, using the kinetic data in Figure 13a. With red-edge pumping, the initial excitation is largely ν_{OH}^R, with the ν_{OH}^B buildup resulting primarily from the interconversion process $\nu_{OH}^R \rightarrow \nu_{OH}^B$ with rate constant k_{inter}. The kinetic equations in this case would be

$$\frac{d}{dt}[\nu_{OH}^R] = -(k_R - k_{inter})[\nu_{OH}^R] + P(t)$$

$$\frac{d}{dt}[\nu_{OH}^B] = k_{inter}[\nu_{OH}^R] - k_B[\nu_{OH}^B] \quad (1)$$

where $(k_R)^{-1} = 0.5$ ps and $(k_B)^{-1} = 0.8$ ps are the lifetimes, and $P(t)$ is the 0.55 ps hwhm apparatus time response function. We fit the data in Figure 13a by varying the value of k_{inter}. Increasing or decreasing $k_{inter} \ll k_R$ or k_B affects primarily the relative amplitudes of the ν_{OH}^R and ν_{OH}^B populations. The best fit was obtained with $(k_{inter})^{-1} = 2$ ps.

Another approach to the interconversion process is to look at literature values for orientational relaxation time constants. Woutersen et al. give[12] ~0.7 ps on the blue edge and ~10 ps on the red edge, and Laenen et al., while differing on specifics, give similar values.[3] This seems to imply $\nu_{OH}^R \rightarrow \nu_{OH}^B$ interconversion cannot be faster than 10 ps, as opposed to the 2 ps we estimate. This 10-ps value may be correct, but we wish to point out how difficult it is to accurately measure 10-ps time constants in a system with a <1-ps lifetime, so we suspect that the 10-ps value might be an overestimate.

C. Origin of the Two Subbands. Since our experiments reveal that the ν_{OH}^R and ν_{OH}^B subbands have different dynamics, we will first concentrate on understanding the mechanism of dynamical distinguishability, and discuss structural distinguishability next. The most significant feature that distinguishes ν_{OH}^R is a greater coupling to the bending vibration, which opens up additional VR channels, and enhances the VR rate. The specific coupling at issue, a stretch-to-bend coupling $V_{\nu\rightarrow\delta}^{(n)}$, is an *n*-th order matrix element[61] of the anharmonic potential,

$$V_{\nu\rightarrow\delta}^{(n)} = \frac{1}{n!}\frac{\partial^n V(Q,q)}{\partial Q_\nu\, \partial Q_\delta\, \partial q_1 ... \partial q_{n-2}}\bigg|_{\{Q,q=0\}} Q_\nu Q_\delta q_1 ... q_{n-2} \quad (2)$$

In eq 2, Q represents intramolecular vibration coordinates for

stretches (Q_ν) and bends (Q_δ), q represents bath vibration coordinates, and $V(Q,q)$ is the potential surface.[61] The operator in eq 2 allows various combination bands and overtones $Q_\delta q_1 ... q_{n-2}$ of the bath to exert fluctuating forces on Q_ν that give rise to processes that annihilate the stretch ν_{OH} and create a bending excitation plus $n - 2$ bath excitations. The bath excitations include hydrogen bond torsions and stretches and excitations of the continuum of lower frequency collective states. On the basis of what we know about VR in other systems, it seems likely that the most efficient $\nu_{OH} \rightarrow \delta_{H_2O}$ transitions involve torsions τ. In water a torsion transition can be observed in the IR at 675 cm^{-1}, with a substantial density of states throughout the 450−950-cm^{-1} region. Hydrogen bond stretches ν_{HB} are observed near 180 cm^{-1}. Thus some representative and likely $\nu_{OH} \rightarrow \delta_{H_2O}$ transitions might be

$$\nu_{OH}(3200\ cm^{-1}) \rightarrow \delta_{H_2O}(1640\ cm^{-1}) + 2\tau(780\ cm^{-1})$$

which involves a quartic ($n = 4$) coupling matrix element, or

$$\nu_{OH}(3200\ cm^{-1}) \rightarrow \delta_{H_2O}(1640\ cm^{-1}) + \nu_{HB}(180\ cm^{-1}) + 2\tau(690\ cm^{-1})$$

which involves an $n = 5$ matrix element.

There is also another operator similar to eq 2 having *a pair* of Q_δ coordinates that results in the creation of $2\delta_{H_2O}$ plus $n - 3$ bath excitations. We have previously demonstrated that ν_{OH} decay in water produces no detectable[27] $2\delta_{H_2O}$, so this term is not needed to describe water. Although preliminary results on HOD/D_2O indicate that some $2\delta_{HOD}$ is produced, the extension of the anharmonic coupling model to include this process is straightforward and will not be discussed further.

We can think of two general types of explanations[22] for the enhanced $V^{(n)}_{\nu\rightarrow\delta}$ coupling in ν^R_{OH} relative to ν^B_{OH}: (1) in the red-shifted ν^R_{OH} subband $V^{(n)}_{\nu\rightarrow\delta}$ coupling is enhanced due to a smaller energy splitting between the stretch and the bend or bend overtone, or (2) the $V^{(n)}_{\nu\rightarrow\delta}$ coupling is enhanced in ν^R_{OH} as a result of local environments that favor stronger anharmonic coupling of the stretch with the bend or bend overtone and certain bath vibrations. The first possibility may be termed an *energy splitting argument*, the second possibility a *configuration argument*.

Some insights into the nature of the subbands can be gained by comparing HOD/D_2O and water. In Figure 17 we have plotted the Raman spectra of both isotopomers along with Gaussian approximations of the Raman spectra of the two subbands ν^R_{OH} and ν^B_{OH}. Since the subband peaks and widths vary with time, there is some latitude in how to do this, so we tried to approximate the equilibrium spectra of the subbands by using the longer time parameters from Figure 11. Figure 17 makes an important point. The ν^R_{OH} subbands in both water and HOD/D_2O have *almost the same spectrum* (peak maximum, fwhm) *and similar dynamics* (VR lifetime, VR pathways); however, in HOD/D_2O ν^R_{OH} has *a much smaller amplitude*.

The red-shifted ν^R_{OH} subband with its enhanced $V^{(n)}_{\nu\rightarrow\delta}$ coupling should be associated with configurations having stronger hydrogen bonding, and these might well be what are termed "ice-like" configurations. This association is strengthened due to the strong resemblance of ν^R_{OH} to the spectrum of the subband in Figure 3 denoted I by Lawrence and Skinner.[29] An additional connection can be made by noting that the ν_{OH} lifetime in HOD/D_2O (in our language this refers to the dominant ν^B_{OH} subband) is known to drop suddenly[13] from 0.7 to 0.4 ps when the HOD/D_2O freezes into ice. We believe these conclusions, that the ν^R_{OH} subbands in water and HOD/D_2O are almost identical except for amplitude and that the red-shifted spectrum and shorter lifetime of ν^R_{OH} should be associated with ice-like structures, are keys to help understand the structural origin of the subbands.

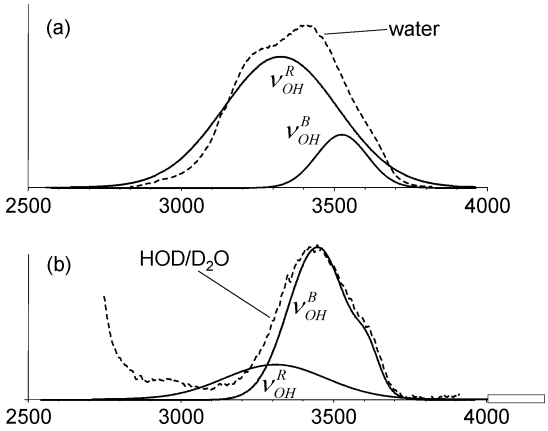

Figure 17. Spectra (Gaussian approximation) of the two vibrational subbands ν^R_{OH} and ν^B_{OH} of water and HOD/D_2O ($\upsilon = 1 \rightarrow 0$ transitions) compared to the Stokes Raman spectra ($\upsilon = 0 \rightarrow 1$ transition; dashed curves). We used the longer time peak locations and fwhm data from Figure 12 to calculate the subband spectra. The ν^R_{OH} subbands in water and HOD/D_2O are quite similar except for the greater amplitude in water. The ν^B_{OH} subband of HOD/D_2O is broader and red shifted compared to water.

These conclusions appear to rule out the energy mismatch argument because while the ν^R_{OH} properties are similar in water and HOD/D_2O, the mismatch is different. The stretch-to-bend mismatch is about 200 cm^{-1} larger in HOD/D_2O and the stretch-to-(bend overtone) mismatch is completely different: in water ν_{OH} and $2\delta_{H_2O}$ are resonant, but in HOD/D_2O ν_{OH} and $2\delta_{HOD}$ are split. In the water-to-ice lifetime measurement of Woutersen and Bakker,[13] freezing affects the configuration but not the energy mismatch, seemingly confirming that the lifetime difference between ν^B_{OH} and ν^R_{OH} can result from a structural change from a liquid-like to an ice-like environment.

Owing to the difficulties in making structural interpretations with use of vibrational spectroscopy alone,[31,36] this section is necessarily brief. Stronger "ice-like" hydrogen bonding appears to be associated with enhanced $V^{(n)}_{\nu\rightarrow\delta}$ coupling. A difficult issue is why the ν^R_{OH} subband amplitude is lower in HOD/D_2O relative to water. We do not yet have a convincing explanation for this. However, we think the focus should be on one notable difference between the two systems. In HOD/D_2O ν_{OH} is a single excitation mainly localized on the OH moiety whereas in water there are two different kinds (symmetric and antisymmetric) of ν_{OH} vibrations, both delocalized over the entire molecule. How these delocalized vibrations lead to greater anharmonic coupling we can only speculate. Possibly the amplitude of ν^R_{OH} is greater in water because there are more ways that ν_{OH} can participate in strong hydrogen bonding (the O-atom and both H-atoms) than in HOD/D_2O (the O-atom and only one H-atom).

5. Conclusion

We have shown that two dynamically distinguishable contiguous spectral regions (subbands) exist within the band of ν_{OH} excitations in $\upsilon = 1$ of both water and HOD/D_2O. These two main features, termed ν^R_{OH} and ν^B_{OH}, evidence stronger or weaker anharmonic coupling between the stretch and bend

excitations. The two subbands overlap a great deal, and interconvert slowly (2−10 ps) compared to the VR lifetime (∼1 ps). As a result of enhanced $V^{(n)}_{\nu\rightarrow\delta}$ coupling, ν^{R}_{OH} has additional decay pathways that ν^{B}_{OH} does not, leading to a shorter lifetime for ν^{R}_{OH}. Our confidence in these distinct subbands, whose existence and number has been controversial until now, stems from our use of anti-Stokes Raman scattering rather than the more usual IR transmission method to probe water excitations. With Raman we are able to simultaneously observe both the decay of the parent ν_{OH} excitation and the generation of bending vibration daughters. These observations, made as a function of pump frequency, clearly demonstrate the existence of two dynamically distinguishable subbands.

The spectra and vibrational dynamics of the red-shifted ν^{R}_{OH} subbands are quite similar in water and HOD/D_2O, even though the energy gaps between stretching and bending vibrations are quite different. This shows that the enhanced $V^{(n)}_{\nu\rightarrow\delta}$ coupling in ν^{R}_{OH} is not a result of local structural environments that reduce the stretch-to-bend energy gap. Thus the differences that lead to two distinct subbands appear not to be energetic, but rather structural in nature. Since the ν^{R}_{OH} subband is red shifted and has a spectrum similar to the "ice-like" component seen in water simulations, and since both ν^{R}_{OH} and ice have shorter lifetimes, it is natural to associate the ν^{R}_{OH} subband with ice-like structures and the ν^{B}_{OH} subband with the remaining structures having weaker hydrogen bonding. It is difficult to explain why the ν^{R}_{OH} subband has a smaller amplitude in HOD/D_2O than in water. We believe the explanation lies in the different nature of stretching vibrations in water and in HOD. In water there are two stretching vibrations delocalized over the entire molecule whereas in HOD there is only one stretch localized on the OH moiety.

Acknowledgment. This material is based on work supported by the National Science Foundation under award No. DMR-0096466, by Army Research Office contract DAAD19-00-1-0036, and by Air Force Office of Scientific Research contract F49620-03-1-0032.

References and Notes

(1) Laubereau, A.; Kaiser, W. *Rev. Mod. Phys.* **1978**, *50*, 607.
(2) Rice, S. A. Conjectures on the structure of amorphous solid and liquid water. In *Topics in Current Chemistry*; Schuster, P., et al., Eds.; Springer: New York, 1975; Vol. 60, p 109.
(3) Laenen, R.; Rauscher, C.; Laubereau, A. *J. Phys. Chem. B* **1998**, *102*, 9304.
(4) Laenen, R.; Rauscher, C.; Laubereau, A. *Phys. Rev. Lett.* **1998**, *80*, 2622.
(5) Wernet, P.; Nordlund, D.; Bergmann, U.; Cavalleri, M.; Odelius, M.; Ogasawara, H.; Näslund, L. A.; Hirsch, T. K.; Ojamäe, L.; Glatzel, P.; Pettersson, G. M.; Nilsson, A. *Science* **2004**, *304*, 995.
(6) Fayer, M. D. *Ultrafast Infrared and Raman Spectroscopy*; Marcel Dekker: New York, 2000.
(7) Mukamel, S. *Principles of Nonlinear Optical Spectroscopy*; Oxford University Press: New York, 1995.
(8) Bakker, H. J.; Nienhuys, H.-K.; Gallot, G.; Lascoux, N.; Gale, G. M.; Leicknam, J.-C.; Bratos, S. *J. Chem. Phys.* **2002**, *116*, 2592.
(9) Bakker, H. J.; Nienhuys, H.-K. *Science* **2002**, *297*, 587.
(10) Kropman, M. F.; Nienhuys, H.-K.; Woutersen, S.; Bakker, H. J. *J. Phys. Chem. A* **2001**, *105*, 4622.
(11) Nienhuys, H.-K.; Woutersen, S.; van Santen, R. A.; Bakker, H. J. *J. Chem. Phys.* **1999**, *111*, 1494.
(12) Woutersen, S.; Emmerichs, U.; Bakker, H. J. *Science* **1997**, *278*, 658.
(13) Woutersen, S.; Emmerichs, U.; Nienhuys, H.-K.; Bakker, H. J. *Phys. Rev. Lett.* **1998**, *81*, 1106.
(14) Woutersen, S.; Bakker, H. J. *Phys. Rev. Lett.* **1999**, *83*, 2077.
(15) Woutersen, S.; Bakker, H. J. *Nature* **1999**, *402*, 507.
(16) Bratos, S.; Gale, G. M.; Gallot, G.; Hache, F.; Lascoux, N.; Leicknam, J.-C. *Phys. Rev. E* **2000**, *61*, 5211.
(17) Gale, G. M.; Gallot, G.; Hache, F.; Lascoux, N.; Bratos, S.; Leicknam, J.-C. *Phys. Rev. Lett.* **1999**, *82*, 1068.
(18) Gale, G. M.; Gallot, G.; Lascoux, N. *Chem. Phys. Lett.* **1999**, *311*, 123.
(19) Gallot, G.; Lascoux, N.; Gale, G. M.; Leicknam, J.-C.; Bratos, S.; Pommeret, S. *Chem. Phys. Lett.* **2001**, *341*, 535.
(20) Fecko, C. J.; Eaves, J. D.; Loparo, J. J.; Tokmakoff, A.; Geissler, P. L. *Science* **2003**, *301*, 1698.
(21) Vodopyanov, K. L. *J. Chem. Phys.* **1991**, *94*, 5389.
(22) Deàk, J. C.; Iwaki, L. K.; Dlott, D. D. *J. Phys. Chem.* **2000**, *104*, 4866.
(23) Wang, Z.; Pang, Y.; Dlott, D. D. *J. Chem. Phys.* **2004**, *120*, 8345.
(24) Lock, A. J.; Woutersen, S.; Bakker, H. J. *J. Phys. Chem. A* **2001**, *105*, 1238.
(25) Lock, A. J.; Bakker, H. J. *J. Chem. Phys.* **2002**, *117*, 1708.
(26) Pakoulev, A.; Wang, Z.; Dlott, D. D. *Chem. Phys. Lett.* **2003**, *371*, 594.
(27) Pakoulev, A.; Wang, Z.; Pang, Y.; Dlott, D. D. *Chem. Phys. Lett.* **2003**, *380*, 404.
(28) Wang, Z.; Pakoulev, A.; Pang, Y.; Dlott, D. D. *Chem. Phys. Lett.* **2003**, *378*, 281.
(29) Lawrence, C. P.; Skinner, J. L. *Chem. Phys. Lett.* **2003**, *369*, 472.
(30) Lawrence, C. P.; Skinner, J. L. *J. Chem. Phys.* **2003**, *118*, 264.
(31) Møller, K. B.; Rey, R.; Hynes, J. T. *J. Phys. Chem. A* **2004**, *108*, 1275.
(32) Rahman, A.; Stillinger, F. H. *J. Chem. Phys.* **1971**, *55*, 3336.
(33) Luzar, A.; Chandler, D. *Nature* **1996**, *379*, 55.
(34) Stern, H. A.; Berne, B. J. *J. Chem. Phys.* **2001**, *115*, 7622.
(35) Luzar, A.; Chandler, D. *Phys. Rev. Lett.* **1996**, *76*, 928.
(36) Rey, R.; Møller, K. B.; Hynes, J. T. *J. Phys. Chem. A* **2002**, *106*, 11993
(37) Lawrence, C. P.; Skinner, J. L. *J. Chem. Phys.* **2002**, *117*, 5827.
(38) Lawrence, C. P.; Skinner, J. L. *J. Chem. Phys.* **2003**, *119*, 1623.
(39) Lawrence, C. P.; Skinner, J. L. *J. Chem. Phys.* **2002**, *117*, 8847.
(40) Lawrence, C. P.; Skinner, J. L. *J. Chem. Phys.* **2003**, *119*, 3840.
(41) Rey, R.; Hynes, J. T. *J. Chem. Phys.* **1996**, *104*, 2356.
(42) Rey, R.; Møller, K. B.; Hynes, J. T. *Chem. Rev.* **2004**, *104*, 1915.
(43) Herzberg, G. *Molecular Spectra and Molecular Structure II. Infrared and Raman Spectra of Polyatomic Molecules*; Van Nostrand Reinhold: New York, 1945.
(44) Besnard, M.; Danten, Y.; Tassaing, T. *J. Chem. Phys.* **2000**, *113*, 3741.
(45) Hadži, D.; Bratos, S. *The Hydrogen Bond*; Elsevier: Amsterdam, The Netherlands, 1976.
(46) Novak, A. *Struct. Bonding* (*Berlin*) **1974**, *18*, 177.
(47) Bratos, S.; Leicknam, J.-C. *J. Chem. Phys.* **1994**, *101*, 4536.
(48) Nibbering, E. T. J.; Elsaesser, T. *Chem. Rev.* **2004**, *104*, 1887.
(49) Deàk, J. C.; Iwaki, L. K.; Rhea, S. T.; Dlott, D. D. *J. Raman Spectrosc.* **2000**, *31*, 263.
(50) Iwaki, L. K.; Deàk, J. C.; Rhea, S. T.; Dlott, D. D. Vibrational energy redistribution in polyatomic liquids: Ultrafast IR−Raman spectroscopy. In *Ultrafast Infrared and Raman Spectroscopy*; Fayer, M. D., Ed.; Marcel Dekker: New York, 2000.
(51) Dlott, D. D. *Chem. Phys.* **2001**, *266*, 149.
(52) Hofmann, M.; Graener, H. *Chem. Phys.* **1995**, *206*, 129.
(53) Deàk, J. C.; Iwaki, L. K.; Dlott, D. D. *Chem. Phys. Lett.* **1998**, *293*, 405.
(54) Pakoulev, A.; Wang, Z.; Pang, Y.; Dlott, D. D. *Chem. Phys. Lett.* **2004**, *385*, 332.
(55) Piletic, I. R.; Gaffney, K. J.; Fayer, M. D. *J. Chem. Phys.* **2003**, *119*, 423.
(56) Deàk, J. C.; Iwaki, L. K.; Dlott, D. D. *Opt. Lett.* **1997**, *22*, 1796.
(57) Kauranen, M.; Persoons, P. *J. Chem. Phys.* **1996**, *104*, 3445.
(58) Terhune, R. W.; Maker, P. D.; Savage, C. M. *Phys. Rev. Lett.* **1965**, *14*, 681.
(59) Held, H.; Lvovsky, A. I.; Wei, X.; Shen, Y. R. *Phys. Rev. B* **2002**, *66*, 205110.
(60) Bakker, H. J.; Lock, A. J.; Madsen, D. *Chem. Phys. Lett.* **2004**, *385*, 329.
(61) Kenkre, V. M.; Tokmakoff, A.; Fayer, M. D. *J. Chem. Phys.* **1994**, *101*, 10618.